Available online at www.sciencedirect.com
SCIENCE DIRECT®
Journal of Electroanalytical Chemistry 569 (2004) 111–119
Journal of Electroanalytical Chemistry
www.elsevier.com/locate/jelechem

Ion transport through polyelectrolyte multilayers under steady-state conditions

V. García-Morales [a], T.H. Silva [b], C. Moura [b], J.A. Manzanares [a,*], F. Silva [b]

[a] *Departament de Termodinàmica, Universitat de València, E-46100 Burjassot, Spain*
[b] *LEQA – Laboratório de Electroquímica e Química Analítica CIQ-L4 Departamento de Química, Faculdade de Ciências do Porto, Rua do Campo Alegre, 687, 4169-007 Porto, Portugal*

Received 2 October 2003; received in revised form 12 February 2004; accepted 13 February 2004
Available online 9 April 2004

Abstract

The permeability of a self-assembled polyelectrolyte multilayer to small ions under the influence of an applied potential difference is studied as a function of the number of layers and the nature of the supporting electrolyte. The multilayer is described as a series of homogeneously charged membranes with alternating sign of their fixed charge. Ion transport is described on the basis of the diffusion equation and the assumption of (Donnan) electrochemical equilibrium at the boundaries between layers. The calculated steady-state current–voltage curves are found to be in good agreement with experimental linear sweep voltammograms (at low sweep rate). The permeability of polystyrenesulfonate/polyallylamine multilayers to ferro/ferricyanide ions is found to decrease monotonically with increasing number of layers when sodium perchlorate is used as the supporting electrolyte. However, an interesting non-monotonic dependence on the number of layers is observed when the supporting electrolyte is barium perchlorate. Both types of behaviour are accounted for satisfactorily by the theoretical model.

Keywords: Membrane-covered electrode; Polyelectrolyte multilayers; Linear sweep voltammetry; Supporting electrolyte; Theory

1. Introduction

Self-assembled polyelectrolyte multilayers (PEMUs) can be obtained by sequential adsorption of polymers of two or more types in a solid substrate [1]. These novel materials have proven applications in several areas including light-emitting diodes [2], nonlinear optical devices [3–5], biosensors [6–8], gas separation [9], ethanol–water pervaporation [10], electrochromics [11], conductive coatings [12] and patterning [13,14]. PEMUs have also shown promise as selective membranes for the immobilization of macromolecules or particles [15–20] and for the controlled transport and release of small molecules [21,22].

The build-up of PEMUs is driven by electrostatic interactions between each new layer added and that previous already deposited having a net charge of opposite sign (mainly distributed at the surface). Therefore, each layer of polymer being added reverses the net charge on the surface leaving it primed for the next [1,23]. Several issues concerning this build-up process are currently under debate. For instance, it is not well known to what extent the excess of charge is distributed on the surface. Some studies attribute it to the first few layers under the surface [23,24], while others attribute it to molecule–molecule and molecule–surface charge overcompensation [25,26].

Another aspect that remains to be clarified concerns whether the compensation of the internal charge inside the multilayer "as formed" is due to a 1:1 stoichiometry of the alternating polymers ("intrinsic compensation") or to the presence of mobile salt ions ("extrinsic compensation"); see [27] and references therein. It is generally accepted, however, that if the multilayer is immersed in an external solution with a significant salt concentration, the chemical potential of the salt forces some swelling of the multilayer thus establishing some degree of extrinsic compensation [24,28,29]. The

* Corresponding author. Tel.: +34-96-354-3119; fax: +34-96-354-3385.
E-mail address: manzanar@uv.es (J.A. Manzanares).

0022-0728/$ - see front matter © 2004 Elsevier B.V. All rights reserved.
doi:10.1016/j.jelechem.2004.02.018

importance of this compensation is the subject of a presently raging controversy [27]. In any case, the salt concentration in solution has been proven to be a crucial experimental variable not only in controlling the build-up of the multilayers but also in determining their transport properties [30–35]. The nature of the salt is also relevant: when it is composed of multivalent ions, a strong Donnan exclusion (inclusion) effect is expected for these ions in layers with matching (opposite) charge sign [36]. A detailed knowledge of all these issues is mandatory for the understanding of charge and mass transport properties through PEMUs.

The structure and properties of these PEMUs have been extensively studied by X-ray [1,37] and neutron reflectivity [1,37], ellipsometry [27,38], the quartz crystal microbalance, scanning electron microscopy and atomic force microscopy [39]. Measurements of the ζ potential [40,41] have shown a symmetrical oscillation from -20 mV for the anionic layer to $+20$ mV for the cationic layer. This indicates that during the successive deposition of PSS and PAH layers each polyelectrolyte brings with it a net charge which is, in absolute value, the same for the polyanion and the polycation and does not change during the build-up procedure. This also implies that the charge excess of the multilayer does not vary between the deposition of two consecutive PSS and PAH layers [40,41].

In the present work, ion transport through polyelectrolyte multilayers is studied theoretically and experimentally. Linear sweep voltammetry experiments in the presence of supporting electrolyte are carried out on a polystyrenesulfonate (PSS)/polyallylamine (PAH) multilayer deposited on a gold electrode modified with cysteamine (see Fig. 1). The results are analysed with the help of a theoretical model based on a description of the multilayer as a series of homogeneous charged membranes, the assumption of (Donnan) electrochemical equilibrium at the boundaries between layers, and a diffusion transport mechanism within the layers. The framework for this approach is based on previous models that have been successful in explaining the ion-transport selectivity of polyelectrolyte multilayers deposited on porous supports [32–35].

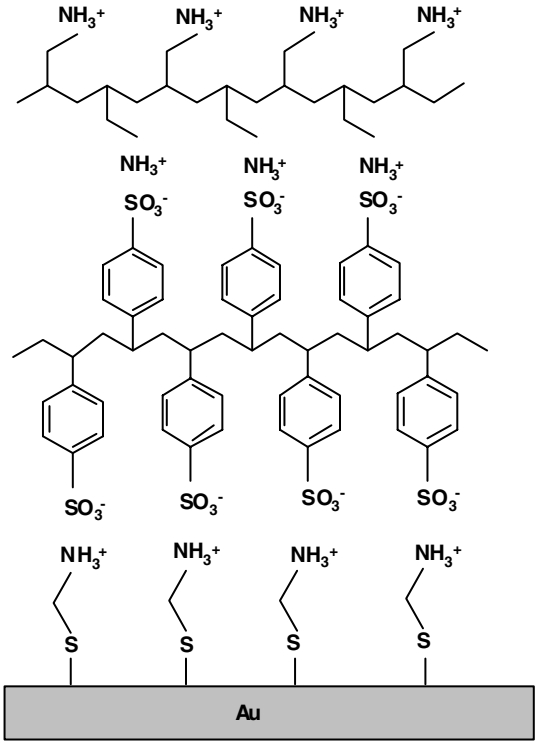

Fig. 1. Scheme of a multilayer Au + cysteamine + PSS + PAH.

2. Theory

The system under study is an isothermal multilayer composed of alternating PAH and PSS layers which is deposited onto a cysteamine-modified working electrode. Following the notation introduced by Silva et al. [42], the total number of bilayers is denoted as $N \equiv (n_{\mathrm{PSS}} + n_{\mathrm{PAH}})/2$, where n_{PSS} and n_{PAH} are the number of layers of PSS and PAH, respectively. Thus, N is an integer number when $n_{\mathrm{PSS}} = n_{\mathrm{PAH}}$ and a semi-integer number when $n_{\mathrm{PSS}} = n_{\mathrm{PAH}} + 1$. The layers are numbered by a superscript running from $i = 0$ for the cysteamine layer to $i = 2N$ for the outer layer in contact with the bulk solution. Layers with even index i are positively charged and layers with odd index are negatively charged. The working electrode is denoted by superscript "e". The molar concentration of fixed charge groups takes the same value $X^i = X$ for layers $i = 0, \ldots, 2N-1$. The charge concentration in these layers can, therefore, be written as $\omega^i X$, where $\omega^i = (-1)^i$ is the charge number of the fixed groups. The concentration of charged groups in the last layer is $X^{2N} = X(1+\alpha)$, where α is a factor describing its relative charge excess. This assumption concerning fixed charge concentration is in agreement with previous experimental findings for PSS/PAH multilayers [40,41] in which the ζ potential was measured indicating always the same oscillation between ± 20 mV.

In every layer a position coordinate x^i running from $x^i = 0$ at the interface with the layer $(i-1)$ to $x^i = d$ at the interface with layer $(i+1)$ is used. The layer thickness d is assumed to be the same for all layers. The charge of the fixed groups in every layer is compensated by the mobile counterions. This assumption is supported by previous experimental results [27,40,43–46]. Moreover, since the multilayers in the system under consideration are bathed by a (moderately) concentrated solution of supporting electrolyte, some coions (i.e., mobile ions of the same sign as the fixed groups) are also present. Thus, the local electroneutrality condition

$$\omega^i X^i + \sum_k z_k c_k^i = 0 \tag{1}$$

is assumed to be valid throughout the system. In Eq. (1), c_k^i denotes the molar concentration of k at any position x^i within the ith layer.

It is well known that PEMUs are not perfectly stratified but fuzzy [1]. In our model we assume that stratification persists as a consequence of the build-up process. In some PEMUs there may also exist defects, such as pinholes, that could play a role in the diffusion. However, since the importance of these defects decreases strongly with increasing number of layers and we study films with more than four layers, it is assumed that diffusion takes place through the compact film and not through pinholes or other defects. It is evident that some degree of polyelectrolyte entanglement and partial intrinsic compensation at the junctions between layers is needed to provide stability to the system. However, as far as the permeability of the multilayer to ion transport and the analysis of experimental linear sweep voltammograms are concerned, it can be assumed that the interfacial regions between layers (where Eq. (1) does not apply) play a negligible role. This is confirmed below by the agreement between theoretical and experimental results.

The boundary conditions at the interfaces between layers are provided by the (Donnan) electrochemical equilibrium condition. Multivalent charged ions, such as those considered in this work, are then expected to be strongly excluded in regions of fixed charge with matching sign. This condition introduces the concept of electrostatic partitioning within the multilayer, which appears to be of special relevance to understand the low permeabilities observed (e.g., of the order of 10^{-4} cm s^{-1} in [36]).

The film-modified working electrode is immersed in a solution containing five ionic species. The electrochemical probe is $[Fe(CN)_6]^{3-/4-}$ which is added to the solution in the form of $K_4Fe(CN)_6$. The supporting electrolyte is either $Ba(ClO_4)_2$ or $NaClO_4$. The ionic species are identified by the following subscripts: $k = 1$ for $Fe(CN)_6^{4-}$, $k = 2$ for K^+, $k = 3$ for $Fe(CN)_6^{3-}$, $k = 4$ for Ba^{2+} or Na^+, and $k = 5$ for ClO_4^-. The bulk solution concentration of the different species are $c_1^b = c_{21}^b$, $c_2^b = 4c_{21}^b + 3c_{23}^b$, $c_3^b = c_{23}^b$, $c_4^b = c_{45}^b$, and $c_5^b = 2c_{45}^b$ ($Ba(ClO_4)_2$) or $c_5^b = c_{45}^b$ ($NaClO_4$), where c_{21}^b and c_{23}^b denote the $K_4Fe(CN)_6$ and $K_3Fe(CN)_6$ concentrations. The supporting electrolyte concentration is c_{45}^b.

The sign convention is such that flux densities and electric current density are positive in the positive x^i direction, i.e. from the working electrode to the bulk solution. Due to the presence of inert supporting electrolyte, the electric potential in every layer is roughly uniform and the electric current density does not significantly modify the potential drops between adjacent layers. The interfacial potential drops are defined as $\Delta_i^{i+1}\phi \equiv \phi^{i+1} - \phi^i$, where $\phi^{2N+1} \equiv \phi^b$ is taken as zero.

Under steady-state conditions, the continuity equation for species k requires that its flux density J_k must take the same value in every layer i. The flux densities of the electroactive ions are $J_1 = -J_3 = -I/F$ and are approximately related to the concentration drop in the layer through the diffusion equation

$$J_k \approx -D_k \frac{dc_k^i}{dx^i} = -\frac{D_k}{d}\left[c_k^i(d) - c_k^i(0)\right]. \tag{2}$$

The flux densities of the inert ions are zero and their concentrations are approximately uniform within all layers.

Eq. (2) shows that the concentration drops of species $k = 1$, 3 are the same in every layer. These ions are counterions in the positively charged PAH layers and coions in the negatively charged PSS layers. The ionic concentrations at both sides of a PAH|PSS interface are not equal to each other, and hence the PAH layers exhibit a higher permeability to these ions than the PSS layers. At the PAH|PSS interfaces all species are assumed to satify the equilibrium condition

$$c_k^i(d)e^{z_k f \phi^i} = c_k^{i+1}(0)e^{z_k f \phi^{i+1}}, \tag{3}$$

where $f \equiv F/RT$. The factor $e^{z_k f \phi^i}$ accounts for the electrostatic partitioning of ionic species k in layer i whose potential with respect to bulk solution is approximately uniform and given by ϕ^i. The permeability of the layer i to species k can be defined as

$$P_k^i = P_k e^{-z_k f \phi^i}, \tag{4}$$

where $P_k \equiv D_k/d$ is the permeability corresponding to a neutral layer. Thus, in a positively charged layer, the electric potential with respect to bulk solution is positive and $e^{-z_k f \phi^i} > 1$ for $k = 1, 3$, while the opposite is true for negatively charged layers. Moreover, since $z_1 = -4$ and $z_3 = -3$, P_k^i and P_k^{i+1} can be very different from each other for $k = 1$ and 3.

When considering the transport across the whole film, the equilibrium condition in Eq. (3) allows us to write

$$\begin{aligned} J_k &= -P_k^T(c_k^b - c_k^s) \\ &= -P_k^T \sum_{i=0}^{2N}\left[c_k^i(d)e^{z_k f \phi^i} - c_k^i(0)e^{z_k f \phi^i}\right] \\ &= P_k^T J_k \sum_{i=0}^{2N} \frac{1}{P_k^i} \end{aligned} \tag{5}$$

and, therefore,

$$\frac{1}{P_k^T} = \sum_{i=0}^{2N} \frac{1}{P_k^i} = \frac{1}{P_k}\sum_{i=0}^{2N} e^{z_k f \phi^i}, \tag{6}$$

where $c_k^b = c_k^{2N}(d)e^{z_k f \phi^{2N}}$ and $c_k^s = c_k^0(0)e^{z_k f \phi^0}$ are the bulk and "surface" concentrations of species k; strictly speaking $c_k^0(0)$ is the surface concentration and c_k^s is the

external concentration in equilibrium with it when the potential in the cysteamine layer is ϕ^0 with respect to the bulk.

Obviously, in the absence of electrostatic partitioning effects, Eq. (6) reduces to $(P_1^T)_n \equiv P_1/(2N+1)$, which is the permeability of a neutral multilayer. However, such a simple expression cannot be used in our system because it predicts much higher limiting currents than those observed experimentally (see below), and this is indirect evidence of the importance of electrostatic partitioning.

The current–voltage curves can be calculated from the polarographic equation

$$E = E_{1/2} + \frac{1}{f}\ln\frac{I}{I_{\lim} - I}, \tag{7}$$

where

$$I_{\lim} = -FAJ_{1,\lim} = FAP_1^T c_1^b, \tag{8}$$

$$E_{1/2} = E^o + \frac{1}{f}\ln\frac{P_1^T}{P_3^T}, \tag{9}$$

are the limiting current (corresponding to $c_1^s = 0$) and the half-wave potential. Eq. (7) can be shown as follows. The electrode potential with respect to the bulk solution is

$$E = \phi^e - \phi^b = \phi^e - \phi^0 + \phi^0 - \phi^b. \tag{10}$$

Since the electrode reaction at the working electrode is $Fe(CN)_6^{4-} \leftrightarrows Fe(CN)_6^{3-} + e^-$, the potential drop across the electrode|cysteamine layer interface is given by the Nernst equation as

$$\phi^e - \phi^0 = E^o + \frac{1}{f}\ln\frac{c_3^0(0)}{c_1^0(0)} \tag{11}$$

and then

$$E = E^o + \frac{1}{f}\ln\left[\frac{c_3^0(0)}{c_1^0(0)}e^{f\phi^0}\right] = E^o + \frac{1}{f}\ln\frac{c_3^s}{c_1^s} = E^\circ + \frac{1}{f}\ln\left(\frac{c_3^s}{c_1^b}\frac{c_1^b}{c_1^s}\right). \tag{12}$$

From Eq. (5), the surface concentrations of the ferrocyanide and ferricyanide ions are given, respectively, by $c_1^s = c_1^b(1 - I/I_{\lim}) = (I_{\lim} - I)/FAP_1^T$ and $c_3^s = I/FAP_3^T$, where we have used $c_3^b \approx 0$. Straightforward substitution of these concentrations in Eq. (12) leads to Eq. (7).

It is important to stress, however, that the use of the relatively simple equation (7) requires the evaluation of the film permeabilities P_1^T and P_3^T from Eq. (6). These permeabilities are not constant but depend on the composition of the bathing solution, the film composition, and even the current. The steady-state current–voltage curves are obtained by imposing a value of the current I. This value is initially very small (compared to $I_{\lim}$). The potential ϕ^i can be evaluated as a sum of interfacial drops

$$\phi^i = -\sum_{j=i}^{2N}\Delta_j^{j+1}\phi = -\sum_{j=i}^{2N}\left(\phi^{j+1} - \phi^j\right) \tag{13}$$

and every interfacial potential drop is determined from Eq. (3) and the local electroneutrality condition, Eq. (1), applied to positions $x^i = 0$ and d. The solution of this equation system starts from the bulk solution where the ionic concentrations are known. The outer interfacial potential drop $\Delta_{2N}^{2N+1}\phi = -\phi^{2N}$ is obtained by solving the algebraic nonlinear equation

$$(-1)^{2N+1}(1+\alpha)X = \sum_{k=1}^{5} z_k c_k^{2N}(d) = \sum_{k=1}^{5} z_k c_k^b e^{-z_k f\phi^{2N}}, \tag{14}$$

which is obtained from Eqs. (1) and (3) for $i = 2N$ and $x^{2N} = d$. The concentrations at $x^{2N} = 0$ are then obtained from Eq. (2), and the procedure continues from $i = 2N - 1$ to $i = 0$ until position $x^0(0)$ is reached. This allows us to evaluate all the potentials ϕ^i ($i = 0, 1, \ldots, 2N$), the permeabilities P_1^T and P_3^T, and hence the steady-state current–voltage curve. The current density is then slowly increased until the limiting current is reached.

3. Experimental

3.1. Materials

The solvent used in all experiments and in all cleaning procedures was ultra pure water (18 $M\Omega\,cm^{-1}$, Millipore). The cationic alkanethiol used to create the initial layer was cysteamine (Fluka). The alternating anionic and cationic polyelectrolytes were, respectively, poly(sodium 4-styrenesulfonate) PSS (MW = 70,000, Aldrich), poly(allylamine hydrochloride) PAH (MW = 15,000, Aldrich). The scheme of the multilayer with the arrangement of the polyelectrolytes is shown in Fig. 1. Supporting electrolyte $Ba(ClO_4)_2$ (Pronalys* AR) and $NaClO_4$ (Merck) and potassium hexacyanoferrate(II) trihydrate (Fluka) were all used without further purification. All electrochemical experiments were performed in a three-electrode cell at room temperature (20 °C) containing a modified gold disc with a diameter of 2 mm (Radiometer EM-EDI-AuD2) as the working electrode connected to a rotating system (Radiometer), a platinum net as counter electrode and a Ag|AgCl 3 M KCl reference electrode, connected to the working volume with a Luggin capillary, against which all potentials are reported. The cell was enclosed in a grounded Faraday cage.

3.2. Methodology

Gold disc electrodes were polished on a polishing cloth (Buehler), rinsed in water and then cleaned by cycling between the potentials −0.3 and 1.5 V vs.

Ag|AgCl in 0.1 M $HClO_4$ solution at a scan rate of 100 mV s^{-1} until reproducible scans were recorded (1 h approximately). Finally, the electrodes were rinsed with water and ethanol. The clean electrodes were immersed in a 3 mM cysteamine ethanolic solution, overnight for approximately 14–16 h. They were then rinsed with ethanol, followed with water. The first polyelectrolyte multilayer was deposited onto a cysteamine-modified electrode from aqueous 0.1 M acetate buffer solution, pH 4.5, containing 1 mg ml^{-1} of PSS, for 20 min and then rinsed with water for 1 min. This procedure was repeated either using PSS or PAH to produce the desired number of layers and contrasts with the procedure described in [47] where two different concentrations of H_2SO_4 were employed to produce the initial positive layer.

3.3. Electrochemical measurements

Linear sweep voltammetry measurements were performed with the electrochemical cell filled first with 0.1 M $Ba(ClO_4)_2$ and 1 mM $K_4Fe(CN)_6$, using an Autolab PSTAT 10 potentiostat, between −0.2 and 0.6 V, using several sweep rates (10–500 mV s^{-1}). The electrochemical probe in these experiments was $Fe(CN)_6^{3-/4-}$. The rotating disc experiments were carried out at several rates between 100 and 4900 rpm, regulated by a Radiometer CTV 101 speed controller. Solutions filling the electrochemical cell were purged with nitrogen for 10 min before each measurement, and the cell was kept under flowing nitrogen for the duration of the experiment. Another series of experiments was carried using a concentration of 0.1 M $NaClO_4$ as supporting electrolyte.

4. Results and discussion

The parameters considered below are the permeability $P_k \equiv D_k/d$, which is assumed to be equal for the two electroactive species, the bulk concentration c_{23}^{b} of the salt $K_3Fe(CN)_6$, and the relative charge excess α of the last layer. The permeability was chosen to match the values for the measured half wave potential $E_{1/2}$ and the limiting current and corresponded to realistic values of the diffusion coefficient and the thickness of each layer [36]. The concentration of supporting electrolyte in all experiments and calculations was 100 times larger than that of $K_4Fe(CN)_6$, that is, $c_{45}^{b} = 100c_{21}^{b}$. The standard electrode potential $E^{\circ} = 300$ mV and the value $1/f = 25$ mV were used. The area of the working electrode was 3.14 mm^2.

4.1. Equilibrium concentration profiles

When there is no transport of electroactive species, the concentrations of all ionic species are constant inside each layer of the multilayer. As indicated above, multivalent ions are expected to be strongly excluded from regions of fixed charge with matching sign. This is confirmed in Fig. 2, which shows the equilibrium concentration profiles calculated from Eqs. (1) and (3) for all ionic species for $N = 2.5$, $c_{45}^{b} = 0.17X$, $c_{23}^{b} = 4.5 \times 10^{-7} c_{21}^{b}$ and $\alpha = 0$. Electrostatic partitioning, however, also causes the concentration of multivalent ions to increase very significantly in those layers where they are counterions (the PAH layers in this case). It is observed that the concentration of the $Fe(CN)_6^{4-}$ and $Fe(CN)_6^{3-}$ ions throughout the multilayer is always smaller than that of the supporting electrolyte ions, and therefore the assumption that their transport takes place mostly by diffusion can still be safely used.

4.2. Current–voltage characteristics using $Ba(ClO_4)_2$ as supporting electrolyte

When a bias potential is applied to the multilayer, some of the PAH|PSS junctions are polarized in the forward direction thus favoring the conductivity of ions, but others are in the reverse direction, strongly limiting the current and rendering it more diffusive. Since the ionic fluxes are continuous through the multilayer (there are no sources or sinks of charge), it is then clearly understood why the PSS layers have a larger influence on the electric current. The calculated current–voltage characteristics provide some interesting insights. In Fig. 3 these characteristics are plotted for multilayers with different numbers of bilayers. The parameter values used are $c_{45}^{b}/X = 0.17$, $c_{45}^{b} = 100c_{21}^{b}$, $c_{23}^{b} = 4.5 \times 10^{-7} c_{21}^{b}$, $\alpha = 0$ and $P_1 = P_3 = 0.1$ cm s^{-1}. The classical sigmoidal shape is obtained for the current–voltage characteristics. We observe that adding a PAH layer to the multilayer has no appreciable effect on the limiting current (a slight

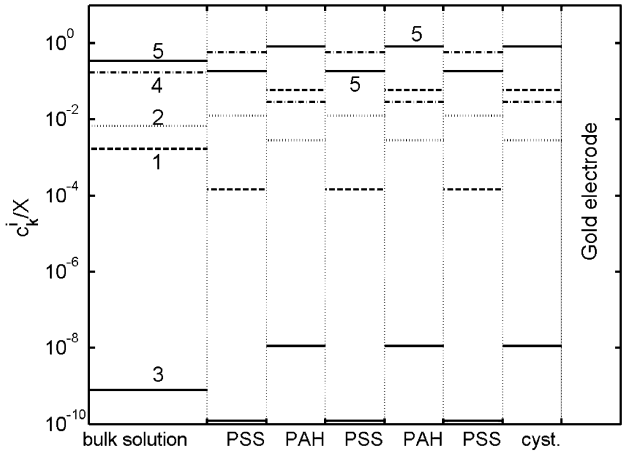

Fig. 2. Equilibrium ionic concentration profiles in a multilayer with $N = 2.5$ bilayers for $c_{45}^{b}/X = 0.17$, $c_{23}^{b} = 4.5 \times 10^{-7} c_{21}^{b}$, and $\alpha = 0$: $Fe(CN)_6^{4-}$ (dashed line, $k = 1$), K^+ (dotted line, $k = 2$), $Fe(CN)_6^{3-}$ (solid line, $k = 3$), Ba^{2+} (dash–dot line, $k = 4$) and ClO_4^- (solid line, $k = 5$).

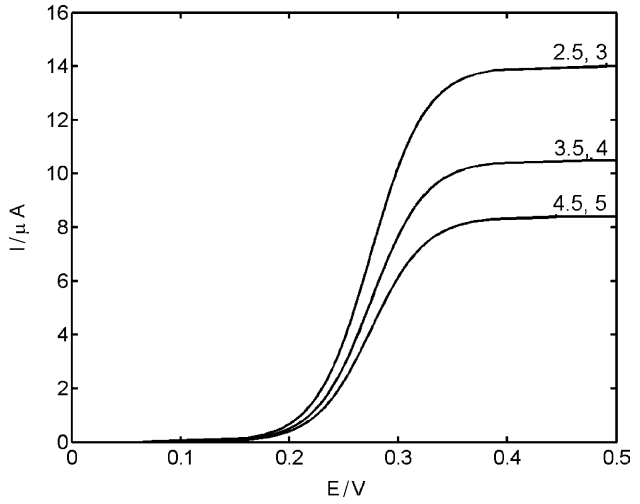

Fig. 3. Calculated steady-state current–voltage curves for the numbers of bilayers N shown on the curves. The supporting electrolyte concentration is $c^{b}_{45}/X = 0.17$ and other parameter values are $c^{b}_{23} = 4.5 \times 10^{-7} c^{b}_{21}$, $\alpha = 0$ and $P_1 = P_3 = 0.1$ cm s^{-1}.

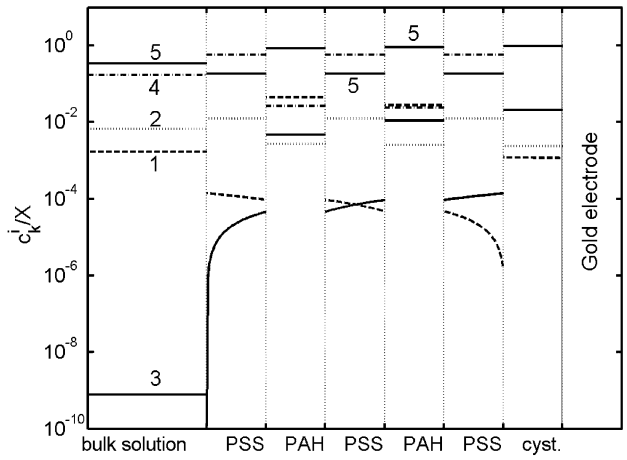

Fig. 4. Ionic concentration profiles in a system of $N = 2.5$ bilayers for $c^{b}_{45}/X = 0.17$, $c^{b}_{23} = 4.5 \times 10^{-7} c^{b}_{21}$, $\alpha = 0$ and $P_1 = P_3 = 0.1$ cm s^{-1} corresponding to an electric current $I = 14.451$ μA close to the limiting value $I_{lim} = 14.483$ μA: $Fe(CN)^{4-}_{6}$ (dashed line, $k = 1$), K^{+} (dotted line, $k = 2$), $Fe(CN)^{3-}_{6}$ (solid line, $k = 3$), Ba^{2+} (dash–dot line, $k = 4$) and ClO^{-}_{4} (solid line, $k = 5$).

decrease was obtained in the calculations, although it is not appreciable in the figure). The half-wave potential $E_{1/2}$ is ca. 0.27 V and remains approximately unchanged when varying the number of layers. This constancy of the half-wave potential is related to the constancy of the ratio P^{T}_{1}/P^{T}_{3} through Eq. (9).

The concentration profiles inside the multilayer for an electric current $I = 14.451$ μA, which is close to the limiting value $I_{lim} = 14.483$ μA, are shown in Fig. 4 and the corresponding interfacial potential drops are given in Table 1. It is interesting to compare Figs. 2 and 4. The interfacial equilibrium remains practically unperturbed for the parameter values considered except at the cysteamine|electrode interface. The concentration of the inert species is constant and that of the active species varies linearly with position within each layer (note the logarithmic scale).

Fig. 5 shows the experimental linear sweep voltammograms of gold-electrodes modified with PSS/PAH multilayers. An interesting feature of the experimental curves is that those with an integer number of bilayers show a higher value for the limiting current than those with a semi-integer number having one less layer deposited. Although Figs. 3 and 5 show similar qualitative trends, this feature of the experimental results is not reproduced by the calculations in Fig. 3.

As indicated above, the excess of charge for PAH/PSS layers has been found not to change after the successive deposition of bilayers. If we suppose an excess of charge homogeneously distributed in the last layer, we can explain the phenomenon described above. A multilayer with a semi-integer number of bilayers brings a negative charge $\omega^{2N} X^{2N} = -X(1+\alpha)$ in the last layer. When another positive layer is deposited on top of it, the charge in the last negative layer is now $-X$. It is because

Table 1
Interfacial potential drops $f\Delta^{i+1}_{i}\phi$ in a system with $N = 2.5$ bilayers for $c^{b}_{45}/X = 0.17$, $c^{b}_{23} = 4.5 \times 10^{-7} c^{b}_{21}$, $\alpha = 0$, $P_1 = P_3 = 0.1$ cm s^{-1}, and electric currents close to $I_{lim}/2$ and to $I_{lim} = 14.483$ μA

Potential drop	$I/I_{lim} = 0.4989$	$I/I_{lim} = 0.9978$
$f\Delta^{cyst}_{e}\phi = f\Delta^{0}_{e}\phi$	−10.40	−14.92
$f\Delta^{PSS1}_{cyst}\phi = f\Delta^{1}_{0}\phi$	−1.57	−1.67
$f\Delta^{PAH1}_{PSS1}\phi = f\Delta^{2}_{1}\phi$	1.54	1.59
$f\Delta^{PSS2}_{PAH1}\phi = f\Delta^{3}_{2}\phi$	−1.54	−1.59
$f\Delta^{PAH2}_{PSS2}\phi = f\Delta^{4}_{3}\phi$	1.52	1.54
$f\Delta^{PSS3}_{PAH2}\phi = f\Delta^{5}_{4}\phi$	−1.52	−1.54
$f\Delta^{bulk}_{PSS3}\phi = f\Delta^{b}_{5}\phi$	0.62	0.62
Total, $fE = -f\Delta^{b}_{e}\phi$	11.35	15.97

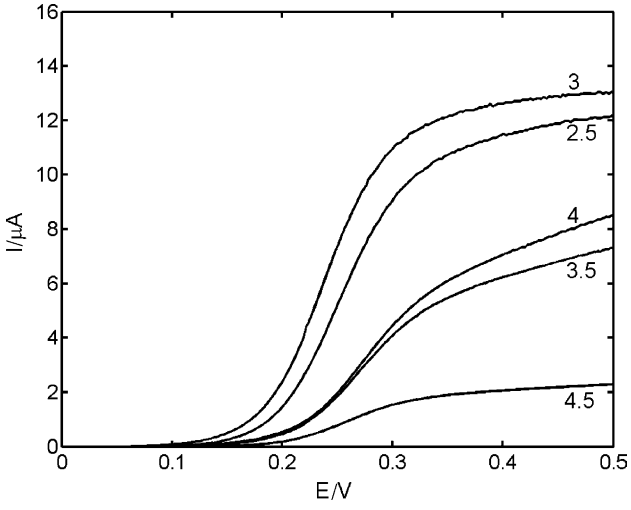

Fig. 5. Experimental linear sweep voltammograms of multilayer-modified rotating disk electrodes for the numbers of bilayers N shown on the curves. Supporting electrolyte: 0.1 M $Ba(ClO_4)_2$, with 1 mM $K_4Fe(CN)_6$. Sweep rate: 10 mV s^{-1}; rotation rate: 900 rpm.

of this compensation of the excess of negative charge by the last positive layer that a higher value for the limiting current is observed for a multilayer with an integer number of bilayers in reference to a multilayer with the immediate lower semi-integer number. This is clearly shown in Fig. 6 where the current–voltage characteristics have now been calculated using a relative excess of charge in the last layer $\alpha = 0.33$. The experimentally observed non-monotonic variation of the limiting current with the number of bilayers is now reproduced by the calculations.

For $N = 3.5$, the theoretical estimation of the permeability of a neutral multilayer to the ferrocyanide ion is $(P_1^{\mathrm{T}})_n = P_1/8 \approx 0.012$ cm s^{-1}. Experimental permeabilities are of the order of 10^{-4} cm s^{-1} [36] and this can be considered as an indirect verification of the importance of the internal electrostatic partitioning. As PSS layers are negatively charged, the actual permeability is $P_1^{\mathrm{T}} \ll (P_1^{\mathrm{T}})_n$. If the fixed charge concentration is reduced and lower permeabilities are considered, the current–voltage characteristics would span the same order of magnitude as those shown in Fig. 5. However, the non-monotonic dependence of the limiting current on N described above requires electrostatic partitioning to be considered.

4.3. Current–voltage characteristics using $NaClO_4$ as supporting electrolyte

The experimental linear voltammograms obtained when using $NaClO_4$ as supporting electrolyte are shown in Fig. 7. It is clearly observed by comparison with Fig. 5, that the nature of the supporting electrolyte strongly influences the permeability of the multilayer, as previously observed in [36]. The ramp-like shape of these voltammograms might be due to a contribution of the

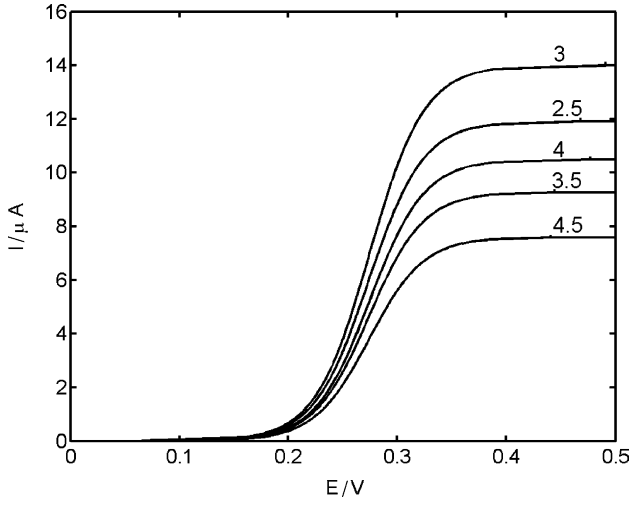

Fig. 6. Calculated steady-state current–voltage curves for the numbers of bilayers N shown on the curves and a relative excess charge in the last layer $\alpha = 0.33$. Other parameter values as in Fig. 3.

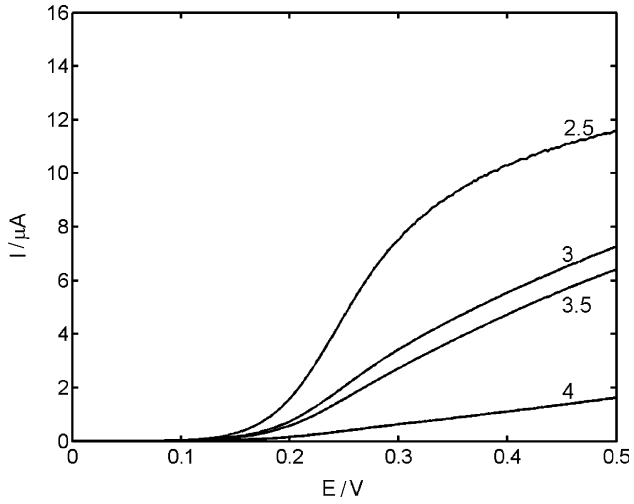

Fig. 7. Experimental linear sweep voltammograms of multilayer-modified rotating disk electrodes for the numbers of bilayers N shown on the curves. Supporting electrolyte: 0.1 M $NaClO_4$, with 1 mM $K_4Fe(CN)_6$; sweep rate: 10 mV s^{-1}; rotation rate: 900 rpm.

electron hopping to the charge transport [30,48]. However, this contribution has not been accounted for in the theoretical model and will not be discussed any further. Instead we concentrate on the fact that the limiting current has now a monotonic dependence on the number of bilayers and that the addition of a single PAH layer (e.g., when varying N from 2.5 to 3) exerts a much stronger influence on the limiting current than observed in Fig. 5. This observation is unexpected because the electroactive species are counterions in the PAH layers and their permeability across these layers should be so large that the addition of a PAH layer to the multilayer should not modify the limiting current significantly. We thus conclude that the probe ions must have a relatively low permeability across the PAH layers and this might be due to an increased thickness of the PAH layers, i.e., the nature of the supporting electrolyte would affect the swelling of these layers. A larger swelling might lead to increased thickness, smaller permeabilities, and then to lower limiting currents as observed in Fig. 8 (see, e.g., the curves for integer N).

Fig. 8 shows the calculated current–voltage curves for $c_{45}^{\mathrm{b}}/X = 2.5$, $c_{23}^{\mathrm{b}} = 4.5 \times 10^{-7} c_{21}^{\mathrm{b}}$, $\alpha = 0$ and $P_1 = P_3 = 1.2 \times 10^{-3}$ cm s^{-1}. These curves are also in qualitative agreement with the experimental observations. A monotonic decrease of the limiting current with increasing N is now observed, in agreement with the experimental findings, because of the relatively low permeability of the layers. Notably, we observe in this case that the neutral permeability of each layer $P_1 = P_3 = 1.2 \times 10^{-3}$ cm s^{-1} leads to a value $(P_1^{\mathrm{T}})_n = P_1/8 = 1.5 \times 10^{-4}$ cm s^{-1} which is of the same order of magnitude as previous experimental values [36]. It should also be mentioned that the observed values for

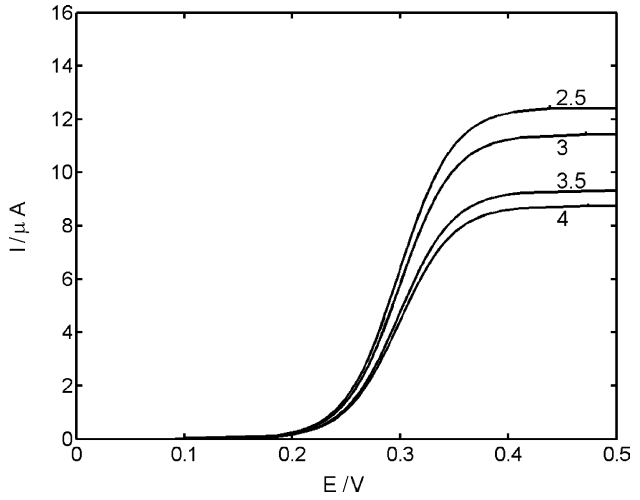

Fig. 8. Calculated steady-state current–voltage curves for the numbers of bilayers N shown on the curves. Other parameter values are $c_{45}^{b}/X = 2.5$, $c_{23}^{b} = 4.5 \times 10^{-7} c_{21}^{b}$, $\alpha = 0$ and $P_1 = P_3 = 1.2 \times 10^{-3}$ cm s^{-1}.

the electric current can be reproduced in the calculated curves only by using relatively high values of the ratio c_{45}^{b}/X (compared to those used in the calculations of Figs. 3 and 6). This supports the hypothesis of increased thickness by swelling. These two facts decrease the role of the electrostatic partitioning in this case.

We observe, however, that some other effects depending on the nature of the supporting electrolyte must be present. The decrease of the electric current due to the addition of a single PAH layer is much larger in the experimental curves than in the calculations. We could tentatively ascribe this to a variation of the diffusion coefficients with the number of layers due to the changes in the compactness and porosity of the multilayer.

5. Conclusions

The permeability of a self-assembled polyelectrolyte multilayer to small ions under the influence of an applied potential difference has been studied as a function of the number of layers and the nature of the supporting electrolyte. The permeability of the multilayer has been described as the appropriate sum of the contribution from the different layers taking into account the electrostatic partitioning.

When using $Ba(ClO_4)_2$ as supporting electrolyte, a non-monotonic decrease of the electric current in the steady-state current–voltage characteristics when increasing the number of layers has been observed. This has been attributed to an excess charge in the more external layer and the effect of the electrostatic partitioning. When using $NaClO_4$, a monotonic decrease of the electric current with increasing N has been observed in the linear sweep voltammograms. In addition, the permeability of the PAH layers was found to be significantly smaller than when $Ba(ClO_4)_2$ was used as supporting electrolyte. This has been attributed to the effect of swelling, leading to a less permeable and thicker multilayer where the effects of electrostatic partitioning are weaker. Although chemical partition coefficients might also be included in the theory (especially in the PAH layers), the calculations have intended to explain only the qualitative behaviour of the system and it has been preferred not to incorporate additional parameters. Indeed, the rather good agreement found between the theoretical current–voltage curves and the experimental linear sweep voltammograms at low scan rate, indicates that both the monotonic and the non-monotonic variation of the current with the number of layers can be accounted for satisfactorily by the theoretical model.

6. List of symbols

Roman symbols

A	area of the bare electrode (cm^2)
c_k^i	concentration of species k within layer i (mol cm^{-3})
c_k^{b}	bulk concentration of species k (mol cm^{-3})
c_{21}^{b}	bulk concentration of $K_4Fe(CN)_6$ (mol cm^{-3})
c_{23}^{b}	bulk concentration of $K_3Fe(CN)_6$ (mol cm^{-3})
c_{45}^{b}	bulk concentration of supporting electrolyte (mol cm^{-3})
c_k^{s}	"surface" concentration of species k (mol cm^{-3})
d	layer thickness (cm)
D_k	diffusion coefficient of species k (cm^2 s^{-1})
E	applied voltage (V)
E^{o}	standard electrode potential (V)
$E_{1/2}$	half wave potential (V)
f	$\equiv F/RT$ (V^{-1})
I	electric current (A)
I_{lim}	limiting current (A)
J_k	flux density of species k (mol cm^{-2} s^{-1})
k	subscript for ionic species: $k = 1$ for $Fe(CN)_6^{4-}$, $k = 2$ for K^+, $k = 3$ for $Fe(CN)_6^{3-}$, $k = 4$ for Ba^{2+} or Na^+, and $k = 5$ for ClO_4^-
N	$\equiv (n_{PSS} + n_{PAH})/2$, number of bilayers
n_{PSS}	number of PSS layers
n_{PAH}	number of PAH layers
P_k	permeability of species k through a neutral layer (cm s^{-1})
P_k^i	permeability of species k through layer i (cm s^{-1})
P_k^{T}	permeability of species k through the multilayer (cm s^{-1})
$(P_k^{T})_n$	permeability of species k through a neutral multilayer (cm s^{-1})
x^i	position coordinate within layer i (cm)
X^i	molar concentration of fixed charge groups in layer i (mol cm^{-3})

Greek symbols

α	relative charge excess
ϕ^i	electrostatic potential in layer i (V)
ϕ^{b}	potential in bulk solution (V)
ϕ^{e}	electrode potential (V)
$\Delta_i^{i+1}\phi$	Donnan potential drop between layers i and $i+1$
ω^i	$=(-1)^i$, charge number of the fixed groups in layer i

Acknowledgements

T.H. Silva gratefully acknowledges the Fundação para a Ciência e a Tecnologia from Portugal for a PhD grant. J.A.M. and V.G.M. are grateful for the financial support from the Ministry of Science and Technology of Spain and the European Funds for Regional Development (FEDER) under Project No. MAT2002-00646. Financial support from the European Union under the research and training network SUSANA (HPRN-CT-2002-00185) is gratefully acknowledged.

References

[1] G. Decher, Science 277 (1997) 1232.
[2] A.C. Fou, O. Onitsuka, M. Ferreira, M.F. Rubner, B.R. Hsieh, J. Appl. Phys. 79 (1999) 7501.
[3] A. Laschewsky, B. Mayer, E. Wischerhoff, X. Arys, P. Bertrand, A. Delcorte, A. Jonas, Thin Solid Films 284 (1996) 334.
[4] M.J. Roberts, G.A. Lindsay, W.N. Herman, K.J. Wynne, J. Am. Chem. Soc. 120 (1998) 11202.
[5] J.R. Heflin, C. Figura, D. Marciu, Y. Liu, R.O. Claus, Appl. Phys. Lett. 74 (1999) 495.
[6] G. Decher, B. Lehr, K. Lowack, Y. Lvov, J. Schmitt, Biosens. Bioelectron. 9 (1994) 677.
[7] Y.M. Lvov, Z. Lu, J.B. Schenkman, J.F. Rusling, J. Am. Chem. Soc. 120 (1998) 4073.
[8] M. Onda, Y. Lvov, K. Ariga, T. Kunitake, Biotechnol. Bioeng. 51 (1996) 163.
[9] J.M. Leväsalmi, T.J. McCarthy, Macromolecules 30 (1997) 1752.
[10] L. Krasemann, B. Tieke, J. Membr. Sci. 150 (1998) 23.
[11] D. Laurent, J.B. Schlenoff, Langmuir 13 (1997) 1552.
[12] J.H. Cheung, A.F. Fou, M.F. Rubner, Thin Solid Films 244 (1994) 985.
[13] P.T. Hammond, G.M. Whitesides, Macromolecules 28 (1995) 7569.
[14] W.T.S. Huck, L. Yan, A. Stroock, R. Haag, G.M. Whitesides, Langmuir 15 (1999) 6862.
[15] E.R. Kleinfeld, G.S. Ferguson, Science 265 (1994) 370.
[16] S. Watanabe, S.L. Regan, J. Am. Chem. Soc. 116 (1994) 8855.
[17] D.L. Feldheim, K.C. Grabar, M.J. Natan, T.C. Mallouk, J. Am. Chem. Soc. 118 (1996) 7640.
[18] Y. Lvov, K. Ariga, M. Onda, I. Ichinose, T. Kunitake, Langmuir 13 (1997) 6195.
[19] N.A. Kotov, I. Dekany, J.H. Fendler, J. Phys. Chem. 99 (1995) 13065.
[20] Y. Sun, X. Zhang, C. Sun, B. Wang, J. Shen, J. Macromol. Chem. Phys. 197 (1996) 147.
[21] P. Stroeve, V. Vasquez, M.A.N. Coelho, J.F. Rabolt, Thin Solid Films 284 (1996) 708.
[22] J.J. Harris, M.L. Bruening, Langmuir 16 (2000) 2006.
[23] J.B. Schlenoff, S.T. Dubas, Macromolecules 34 (2001) 592.
[24] J.B. Schlenoff, H. Ly, M. Ly, J. Am. Chem. Soc. 120 (1998) 7626.
[25] H.G.M. van de Steeg, M.A. Cohen-Stuart, A. de Keizer, B.H. Bijsterbosch, Langmuir 8 (1992) 2538.
[26] S.Y. Park, R.F. Bruinsma, W.M. Gelbart, Europhys. Lett. 46 (1999) 454.
[27] H. Riegler, F. Essler, Langmuir 18 (2002) 6694.
[28] S.T. Dubas, J.B. Schlenoff, Macromolecules 34 (2001) 3736.
[29] S.T. Dubas, J.B. Schlenoff, Langmuir 17 (2001) 7725.
[30] T.R. Farhat, J.B. Schlenoff, Langmuir 17 (2001) 1184.
[31] T.R. Farhat, J.B. Schlenoff, J. Am. Chem. Soc. 125 (2003) 4627.
[32] K. Lebedev, P. Ramírez, S. Mafé, J. Pellicer, Langmuir 16 (2000) 9941.
[33] H. Miyoshi, J. Membr. Sci. 141 (1998) 101.
[34] A.M. Balachandra, J. Dai, M.L. Bruening, Macromolecules 35 (2002) 3171.
[35] M.L. Bruening, D.M. Sullivan, Chem. Eur. J. 8 (2002) 3833.
[36] L. Krasemann, B. Tieke, Langmuir 16 (2000) 287.
[37] R. Steitz, V. Leiner, R. Siebrecht Klitzing, R. von Klitzing, Colloids Surf. A 163 (2000) 63.
[38] J. Ruths, J. Essler, G. Decher, H. Riegler, Langmuir 16 (2000) 8871.
[39] Y. Lvov, K. Ariga, M. Onda, I. Ichinose, T. Kunitake, Colloids Surf. A 146 (1999) 337.
[40] G. Ladam, P. Schaad, J.C. Voegel, P. Schaaf, G. Decher, F. Cuisinier, Langmuir 16 (2000) 1249.
[41] F. Caruso, E. Donath, H. Möhwald, J. Phys. Chem. B 102 (1998) 2011.
[42] T.H. Silva, S.V.P. Barreira, C. Moura, A.F. Silva, Port. Electrochim. Acta 21 (2003) 281.
[43] G.J. Kellog, A.M. Mayes, W.B. Stokton, M. Ferreira, M.F. Rubner, S.K. Satija, Langmuir 12 (1996) 5109.
[44] N.G. Hoogeveen, M.A. Cohen Stuart, G.J. Fleer, Langmuir 12 (1996) 3675.
[45] M. Lösche, J. Schmitt, G. Decher, W.G. Bouwman, K. Kjaer, Macromolecules 31 (1998) 8893.
[46] F. Caruso, H. Lichtenfeld, E. Donath, H. Möhwald, Macromolecules 32 (1999) 2317.
[47] S. Han, B. Lindholm-Sethson, Electrochim. Acta 45 (1999) 845.
[48] S.V.P. Barreira, V. García-Morales, J.A. Manzanares, F. Silva (in preparation).